Available online at www.sciencedirect.com
ScienceDirect
Catalysis Today 131 (2008) 173–178
CATALYSIS TODAY
www.elsevier.com/locate/cattod

Oxidative dehydrogenation of ethylbenzene to styrene with CO_2 over SnO_2–ZrO_2 mixed oxide nanocomposite catalysts

David Raju Burri, Kwang-Min Choi, Dae-Soo Han, Sujandi, Nanzhe Jiang, Abhishek Burri, Sang-Eon Park *

Laboratory of Nano-Green Catalysis and Nano Center for Fine Chemicals Fusion Technology, Department of Chemistry, Inha University, Incheon 402-751, Republic of Korea

Available online 26 November 2007

Abstract

SnO_2–ZrO_2 nanocomposite catalysts with different compositions ranging from 0 to 100% of SnO_2 were prepared at room temperature by co-precipitation method using aqueous ammonia as a hydrolyzing agent. X-ray diffraction, transmission electron microscopic characterization revealed the SnO_2–ZrO_2 nanocomposite behavior. Acid–base properties of these catalysts were ascertained by temperature-programmed desorption (TPD) of NH_3 and CO_2. Both acidic and basic sites distribution of the nanocomposite catalysts is quite different from those of respective single oxides (SnO_2 or ZrO_2). Catalytic activity of these nanocomposite catalysts for ethylbenzene dehydrogenation (EBD) to styrene in the presence of excess CO_2 was evaluated. The change in the acid–base bi-functionality of the nanocomposite catalysts in comparison with single oxides had profound positive influence in enhancing the catalytic activity.

Keywords: Ethylbenzene; Styrene; SnO_2–ZrO_2 nanocomposite catalysts; TPD of NH_3; TPD of CO_2

1. Introduction

Styrene is one of the important commodity chemicals in the petrochemical industry for the production of polystyrene, expandable polystyrene, styrene–butadiene rubber, styrene–butadiene latex and so forth. Based on its wider applications, the demand of styrene has continuously been increasing. The production demand of styrene exceeded 24 million metric tons per annum, of which, more than 90% of its production is from the catalytic dehydrogenation of ethylbenzene over potassium-doped iron oxide catalysts in the presence of excess steam [1,2]. The present commercial process is highly endothermic and volume expanding hence, a large amount of superheated steam has been under use to supply heat, to lower the partial pressure of the product mixture, and to avoid the formation of carbon deposits. However at the gas–liquid separator a large amount of latent heat of steam is being wasted [3]. Consequently, the estimated hike in production cost is about 10% and in addition, development of hotspots, diminishing of catalysts life are inevitable. Among the alternative processes, production of styrene monomer along with propylene oxide is also one of the important processes, wherein ethylbenzene is converted into ethylbenzene hydroperoxide in the presence of oxidizing agents such as hydrogen peroxide or molecular oxygen. Further conversion of ethylbenzene hydroperoxide with propylene leads to propylene oxide and 1-phenyl ethanol. 1-Phenyl ethanol on dehydration produces styrene monomer. In this process styrene production depends on the demand of propylene oxide along with other inevitable problems [4]. The next alternative is the membrane technology, wherein (i) manufacture of highly permeable and resistive membrane, (ii) highly efficient catalyst and (iii) the design of suitable rector are the major constraints [5]. Alternatively, several technological advancements have been emerging recently, of which, oxidative dehydrogenation of ethylbenzene with CO_2 instead of steam has been under intensive investigation [6–13]. However, the dehydrogenation of ethylbenzene process with CO_2 is still in the laboratory scale due to lack of suitable catalysts, which motivated us to explore the possibility of CO_2 utilization on different catalytic systems.

Of late, we have studied the oxidative dehydrogenation of ethylbenzene with CO_2 using ZrO_2 as a catalyst and found that

* Corresponding author. Tel.: +82 32 860 7675; fax: +82 32 867 5604.
E-mail address: separk@inha.ac.kr (S.-E. Park).

0920-5861/$ – see front matter © 2007 Elsevier B.V. All rights reserved.
doi:10.1016/j.cattod.2007.10.031

the acidic and basic sites are indispensable requirement [14]. Latter on, the study has been extended to ZrO_2-based mixed oxide catalysts [15–18]. MnO_2–ZrO_2 mixed oxide catalysts prepared by co-precipitation method exhibited substantial enhancement in the acid–base bi-functionality, which led to higher conversion of ethylbenzene and higher selectivity of styrene in the presence of CO_2 [15]. Similar catalytic behavior has been observed in the case of TiO_2–ZrO_2 mixed oxide catalysts [16]. In both of these catalytic systems, the common observation is that the enhanced acidic and basic sites cooperatively activated CO_2 as well as ethylbenzene under the reaction conditions. In another attempt, CeO_2–ZrO_2 mixed oxide supported SBA-15 catalyst system has been used as a catalyst for the oxidative dehydrogenation of ethylbenzene into styrene with CO_2 [17]. The high performance of this system depends on two factors: (i) enhancement in acid–base bi-functionality and (ii) fine dispersion of CeO_2–ZrO_2 mixed oxide on the support surface. The above results reveal that the mixed oxides are superior to their isolated oxides for the conversion of ethylbenzene in the presence of CO_2 and also smaller particles have superior activity to larger particles. Accordingly, in the present study, SnO_2–ZrO_2 mixed oxide nanocomposite catalysts preparation, characterization and catalytic activity for the dehydrogenation of ethylbenzene to styrene in the presence of CO_2 have been elucidated and furthermore, similar catalytic system has not yet been reported.

2. Experimental

2.1. Preparation of the catalysts

The preparation of SnO_2–ZrO_2 nanocomposite catalysts is based on the co-precipitation method by governing the nucleation and growth process using diluted metal precursor salts. In this synthetic procedure, both the component oxides are mutually contributing for hastening of nucleation and prevention of particle growth. A series of SnO_2–ZrO_2 nanocomposite catalysts were prepared in the full range from 0 to 100% of SnO_2. In a typical preparation, 0.1 M mixed aqueous nitrate or chloride precursor salts solution of each component were prepared under vigorous mechanical stirring at room temperature. Prior to hydrolysis, stirring was continued for a period of 1 h to ensure the formation of homogeneous mixed salt solution. Aqueous ammonium hydroxide solution was added drop wise in a controlled manner in a stretch of 1 h under vigorous stirring until the attainment of required pH (8–9). The stirring was continued for further 2 h and allowed it for 12 h aging at room temperature. The precipitated mixed gel was separated by centrifugation. The mixed hydroxide gel was dried at 100 °C for 12 h and calcined it at 600 °C for 8 h in a muffle furnace in air atmosphere. The catalysts were coded based on the molar percentages. For example 100% SnO_2 catalyst is coded as Sn10Zr0, 100% ZrO_2 is coded as Sn0Zr10 and 10% SnO_2 + 90% ZrO_2 mixed oxide nanocomposite catalyst is denoted as Sn1Zr9, similar pattern was adopted in coding the other catalysts.

A semi-quantitative portable XRF analyzer (Xmet-300, Oxford, UK) is used to estimate the elemental analysis. Inbuilt software directly gives the composition of the elements in weight percent. The weight % of Sn and Zr are converted into mole% assuming 100% yields of SnO_2 and ZrO_2 instead of 99.8 and 98.6, respectively. Small amounts of Hf and Fe are found as impurities in ZrO_2. Similarly, a small amount of Fe is present as impurity in SnO_2.

2.2. Characterization of the catalysts

X-ray diffraction analysis was carried out using Rigaku X-ray diffractometer, model D/max-2200/PC, equipped with a graphite monochromator and Cu Kα radiation (λ = 1.5405 Å) in the 2θ (2 theta) range of 10–80° at a scan speed of 0.5 s, at 40 kV voltage and 20 mA current.

The size, and organization behavior of SnO_2–ZrO_2 nanocomposite catalysts were determined by transmission electron microscopy (TEM) using a Philips 420 transmission electron microscope (TEM) operated at 120 kV and a JEOL-20l0F high-resolution transmission electron microscope (HRTEM) operated at 200 kV. A small amount of the sample was dispersed in absolute ethanol by sonication, and then a drop of this solution was deposited on an amorphous carbon film on 300 mesh Cu grid for TEM observation.

Temperature-programmed desorption (TPD) studies were made using an adsorption unit (Chemisorb-2705) supplied by Micromeritics, USA. The acidity and basicity of the catalysts were determined by TPD of NH_3 and CO_2, respectively. In a typical experiment, c.a 50 mg catalyst sample was pretreated in flowing helium gas at 500 °C for 1 h and allowed it to cool up to 100 °C and at this temperature the pretreated catalyst was exposed to either 5% NH_3 in helium or 10% CO_2 in helium gas mixture with a flow rate of 20 ml/min for 30 min and subsequently the adsorbed NH_3 was purged with helium gas at 100 °C for 1 h to remove the physisorbed NH_3 or CO_2. The chemisorbed amount of either NH_3 or CO_2 was measured in flowing helium gas with the flow rate of 20 ml/min from 100 to 825 °C with the heating rate of 5 °C/min.

2.3. Catalytic performance tests

The catalytic activity studies were performed in a fixed bed down flow stainless steel reactor (i.d. 4.5 mm and length 300 mm) under atmospheric pressure. In a typical experiment, approximately 1.0 g of the catalyst sample was loaded with the support of quartz wool and subjected to the catalyst pretreatment at 600 °C for 0.5 h in the flow of N_2 (20 ml/min). After the completion of the pretreatment, the reaction was conducted at different temperatures either in the flow of N_2 or CO_2. Ethylbenzene was introduced by a peristaltic pump with a feed rate of 8.2 mmol/h along with either CO_2 or N_2. Products were analyzed by a gas chromatogram (Younglin Instrument, Acme 6000 series, Korea) equipped with TCD and FID.

3. Results and discussion

The molar composition of SnO_2 and ZrO_2 in the SnO_2–ZrO_2 nanocomposite catalysts was obtained approximately as

Table 1
Composition of the catalysts after calcinations at 600 °C for 8 h in air

Catalyst code	Catalyst composition (mol%)	
	Sn content	Zr content
Pure SnO_2	99.8	–
Sn1Zr9	10.6	89.4
Sn1.5Zr8.5	13.4	86.6
Sn3Zr7	30.94	69.06
Sn5Zr5	52.9	47.1
Sn9Zr1	91.6	8.4
Pure ZrO_2	–	98.6

calculated based on the yield of the catalysts. The composition of the catalyst was also estimated by XRF and displayed in Table 1. The molar composition (during the preparation step) of the catalysts was given in the code name and the composition of the catalysts obtained by XRF was shown in Table 1.

It is clear from Table 1 that the composition of the catalysts determined by experiment was close to that of taken in the preparation step. Hence, both SnO_2 and ZrO_2 might be precipitated simultaneously during the preparation.

The XRD patterns of SnO_2–ZrO_2 binary mixed metal oxide nanocomposites, SnO_2 (Sn10Zr0) and ZrO_2 (Sn0Zr10) were depicted in Fig. 1. Sn0Zr10 nanocatalyst exhibited sharp diffraction peaks at $2\theta = 24.1$(1 1 0), 28.1(1 1 1), 31.3(1 1 1), 34.1(2 0 0) and 50.2(0 2 2), which are well consistent with the monoclinic phase of ZrO_2 according to the ICDD No. 37-1484. No other crystalline phases of ZrO_2 have been observed. The diffraction lines of Sn10Zr0 are centered at $2\theta = 26.7$(1 1 0), 33.9(1 0 1), 37.9(2 0 0), 51.8(2 1 1) 54.8(2 2 0) and 62.0(3 1 0) are well matched with the rutile cassiterite phase of SnO_2 (JCPDS 41-1445). Both monoclinic phase of ZrO_2 and cassiterite phase of SnO_2 were present in the nanocomposite catalysts containing 10–40% of SnO_2 content, i.e. Sn1Zr9, Sn1.5Zr8.5, Sn2Zr8, Sn3Zr7 and Sn4Zr6 catalysts.

When the content of SnO_2 increased to 50% the XRD pattern is completely different from the ZrO_2-rich nanocomposite catalysts. Fifty to 90% of SnO_2 content nanocomposite

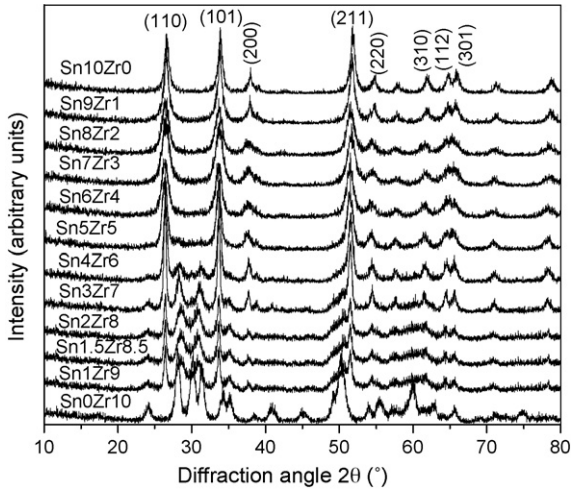

Fig. 1. X-ray diffraction patterns of SnO_2–ZrO_2 catalysts.

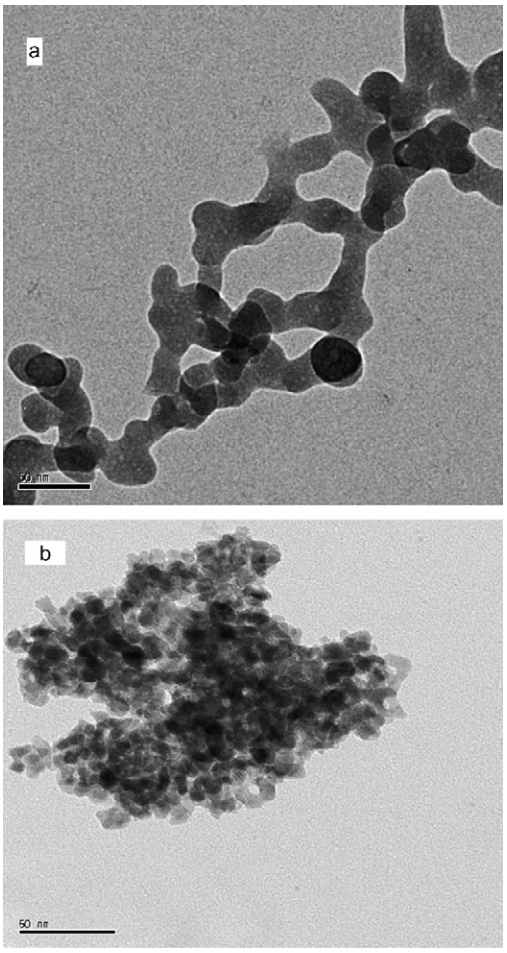

Fig. 2. TEM images of (a) Sn10Zr0 and (b) Sn1.5Zr8.5 catalysts.

catalysts exhibited only cassiterite phase of SnO_2. No significant ZrO_2 XRD reflections were noticed from 50 to 90% SnO_2 content nanocomposites. XRD results of Sn5Zr5, Sn6Zr4, Sn7Zr3, Sn8Zr2 and Sn9Zr1 nanocomposite catalysts suggest two possibilities. The first one is the formation of single-phase solid solution between SnO_2 and ZrO_2 as reported by Ba et al. similar to indium–tin system [19]. The second possibility is the separation of amorphous phase of ZrO_2 from the crystalline phase of SnO_2. The XRD reflections of all the nanocomposite catalysts were broad and less intense, which is an indication of the formation of nanosized crystallites [20].

As a representative example, TEM micrographs of Sn1.5Zr8.5 are shown in Fig. 2. An overview image (Fig. 2) illustrates both individual particles and agglomerates. A closer view on the area with well-dispersed particles demonstrates that the particle size distribution is in the range of 10–15 nm (Fig. 3). The particles are not only characterized by a relatively narrow particle size distribution but also exhibit nearly spherical and uniform particle morphology.

Temperature-programmed desorption (TPD) of NH_3 gives the information about the strength and number of acid sites present in the catalysts. TPD of NH_3 patterns of pure Sn10Zr0, Sn0Zr10 and Sn1.5Zr8.5 catalysts are shown in Fig. 4. It is interesting to see that the reducible SnO_2 has a high-temperature signal ($T_{max} \sim 525$ °C) while the irreducible

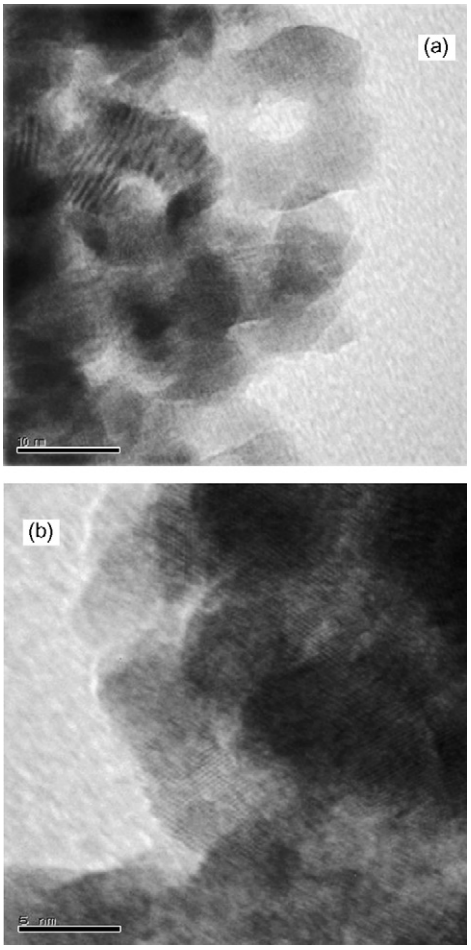

Fig. 3. HRTEM images of Sn1.5Zr8 catalyst at (a) 5 nm and (b) 10 nm magnification.

ZrO_2 has a low-temperature signal ($T_{max} \sim 200$ °C). The high-temperature signal signifies the presence of strong acidic sites and the low-temperature signal indicates the presence of moderate acidic sites. Thus, Sn10Zr0 contains large number of strong acid sites and a very few moderate acid sites ($T_{max} \sim 200$ °C). On the other hand Sn0Zr10 contains good number of moderate acid sites and a very few strong acid sites ($T_{max} \sim 400$, 575 and >600 °C). The signal intensities clearly indicate that the total acidity of Sn0Zr10 is less than that of Sn10Zr0. The TPD of NH_3 pattern of Sn1.5Zr8.5 catalyst exhibits the characteristic features of both SnO_2 and ZrO_2. However, it is surprising to see the more intense low-temperature signal ($T_{max} \sim 225$ °C) than the high-temperature signal ($T_{max} \sim 525$ °C). Also one can observe a slight shifting of low-temperature signal to higher side when compared to that of Sn0Zr10. This is a clear indication of the synergistic effect between SnO_2 and ZrO_2.

The interaction between the two oxides results in a significantly greater surface acidity than that of the single component oxides. As reported in the literature [21], the generation of acidic sites in the mixed oxides is due to the development of negative or positive charge in the model structure. When two transition metals are bonded (M1–O–M2), charge imbalance arises due to electronegativity difference of the contributing two transition metals (M1 and M2), consequently new acidic sites with different strengths will be generated. It is also quite possible that as the transition metal oxide particle size decreases, the numbers of surface oxygen anion vacancies increases, hence new and stronger acid sites are created, with the particles of smallest diameter having the strongest acidity [22].

Temperature-programmed desorption (TPD) of CO_2 gives information about the strength and number of basic sites present in the catalysts. TPD of CO_2 patterns of pure Sn10Zr0, Sn0Zr10 and Sn1.5Zr8.5 catalysts are shown in Fig. 5. TPD of

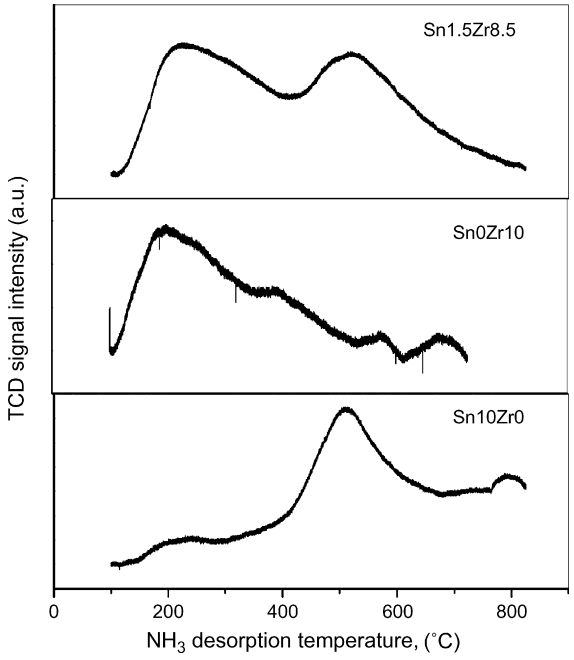

Fig. 4. NH_3 TPD patterns of Sn10Zr0, Sn0Zr10 and Sn1.5Zr8.5 catalysts.

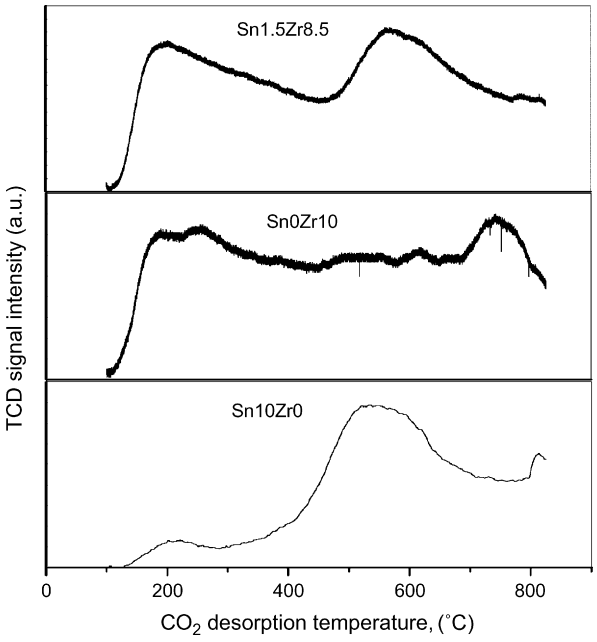

Fig. 5. CO_2 TPD patterns of Sn10Zr0, Sn0Zr10 and Sn1.5Zr8.5 catalysts.

CO_2 pattern of Sn10Zr0 shows the presence of high intense high-temperature signal ($T_{max} \sim 550$ °C) due to strong basic sites and low intense low-temperature signal ($T_{max} \sim 200$ °C) due to weak basic sites. On the other hand, TPD of CO_2 pattern of Sn0Zr10 shows two temperature maxima with more low intense low-temperature signal. The one at a T_{max} of ~200 °C is due to the presence of weak basic sites and other at a T_{max} of ~750 °C is due to the presence of very strong basic sites. The CO_2 TPD pattern of Sn1.5Zr8.5 shows the presence of more or less equal intensities of two temperature maxima one at ~200 °C and the other at a T_{max} of 600 °C. Thus the Sn1.5Zr8.5 catalyst contains the characteristic features of both Sn10Zr0 and Sn0Zr10. The shifting of high-temperature signal to lower temperature compared to that of Sn0Zr10 is again due to the synergistic effect between these two oxides. The acid–base properties of ZrO_2–SnO_2 with different compositions calcined at different temperatures have been reported are more or less similar to cited literature report [23].

As documented in the literature, the dehydrogenation of ethylbenzene to styrene in the presence of CO_2 has beneficial effects than those of inert carriers and steam [6–18]. The beneficial role of CO_2 as a carrier gas and as a mild oxidant has been proved on the SnO_2–ZrO_2 nanocomposite catalyst for the selective conversion of ethylbenzene to styrene with enhanced activity. The catalytic activity behavior with and with out CO_2 has been displayed in Fig. 6. It is clear that there is a clear demarcation in the activity pattern in the presence and absence of CO_2. The higher activity of the catalyst in the presence of CO_2 is believed to be release of equilibrium limitation through coupling of reverse water gas shift reaction with simple dehydrogenation. Hydrogen that produced in the simple dehydrogenation of ethylbenzene (C_6H_5–CH_2–$CH_3 \rightarrow C_6H_5$–CH_2=$CH_2 + H_2$) is oxidized when coupled with reverse water gas shift reaction ($CO_2 + H_2 \rightarrow CO + H_2O$) and there by releases the equilibrium limitation to get higher conversion of ethylbenzene.

Since CO_2 has profound influence on the catalytic activity of SnO_2–ZrO_2 for the dehydrogenation of ethylbenzene to styrene, the optimization of the catalyst composition, reaction temperature and activity of the best catalyst has been compared with single oxides (SnO_2 and ZrO_2) in the presence of CO_2.

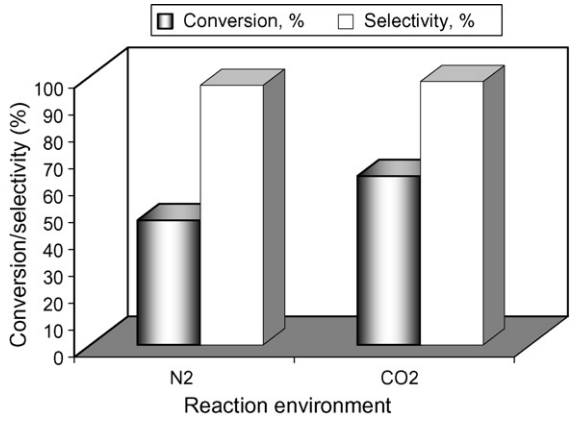

Fig. 6. Influence of CO_2 in the EBD activity over Sn1.5Zr8.5 catalyst. Reaction conditions: catalyst weight = 1.0 g, temperature = 600 °C, pressure = 1 atm, CO_2/EB = 6 (molar ratio), W/F = 17.6 g_{cat} h/mol.

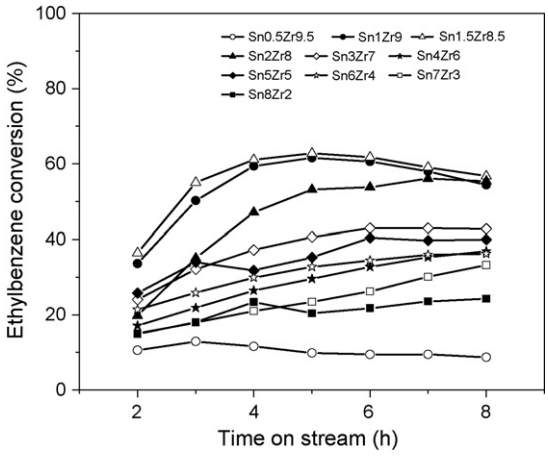

Fig. 7. Ethylbenzene conversion over different loadings of SnO_2–ZrO_2 nanocomposite catalysts. Reaction conditions: catalyst weight = 1.0 g, temperature = 600 °C, pressure = 1 atm, CO_2/EB = 6 (molar ratio), W/F = 17.6 g_{cat} h/mol.

The conversion of ethylbenzene over different compositions of SnO_2–ZrO_2 nanocomposite catalysts with time on stream has been depicted in Fig. 7. The catalytic activity in terms of ethylbenzene conversion over Sn0.5Zr95.5 catalyst is very poor. When SnO_2 content increased from 5 to 10% (Sn1Zr9) the conversion of ethylbenzene has drastically increased and at 15% SnO_2 content catalyst (Sn1.5Zr8.5) the conversion is 61%. Further enhancement in the SnO_2 content from 20 to 80%, the diminishing trend in the conversion of ethylbenzene has been noticed. In spite of low activity of these catalysts (Sn2Zr8 to Sn8Zr2), the time on stream study represent a continuous enhancement in the conversion of ethylbenzene from 2 to 8 h. In the case of Sn1Zr9 and Sn1.5Zr8.5 catalysts, there has been marginal decrease in the conversion of ethylbenzene with time on stream. However, based on the available reaction data the optimum catalyst is Sn1.5Zr8.5 (from XRF data Sn = 13.4% and Zr = 86.6%).

In order to elucidate the catalytic behavior of SnO_2–ZrO_2 nanocomposite catalysts the catalytic activity of Sn1.5Zr8.5 catalyst has been compared with its constituent oxide catalysts (Fig. 8). The conversion of ethylbenzene over bulk SnO_2 (Sn10Zr0) is only 20.6% with the styrene selectivity of 96% and on bulk ZrO_2 (Sn0Zr10) the conversion is 48.8% with the styrene selectivity of 97%, whereas over Sn1.5Zr8.5 nanocomposite catalyst the conversion is 61.1% with 98% styrene selectivity. The superior performance of Sn1.5Zr8.5 nanocomposite catalyst is not surprising. This type of peculiar character of mixed oxides such as TiO_2–ZrO_2, MnO_2–ZrO_2, CeO_2–ZrO_2 have already been reported for the dehydrogenation of ethylbenzene in our earlier reports [15–18]. The peculiarity in the acid–base properties can be seen from Figs. 4 and 5. In the best catalyst (Sn1.5Zr8.5) weak to moderate acidic sites are higher in number than those of isolated ZrO_2 and also strong acidic sites have been generated, which are believed to be originated from the SnO_2 content (Fig. 5). Weak to strong basic sites have been developed, which are higher in number than

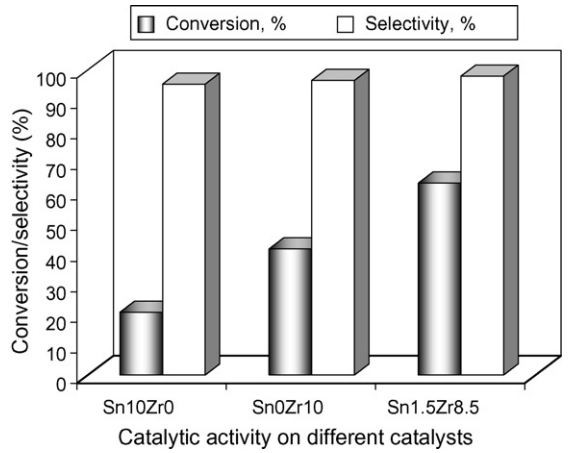

Fig. 8. EBD activity over Sn10Zr0, Sn0Zr10 and Sn1.5Zr8.5 catalysts. Reaction conditions: catalyst weight = 1.0 g, temperature = 600 °C, pressure = 1 atm, CO_2/EB = 6 (molar ratio), W/F = 17.6 g_{cat} h/mol.

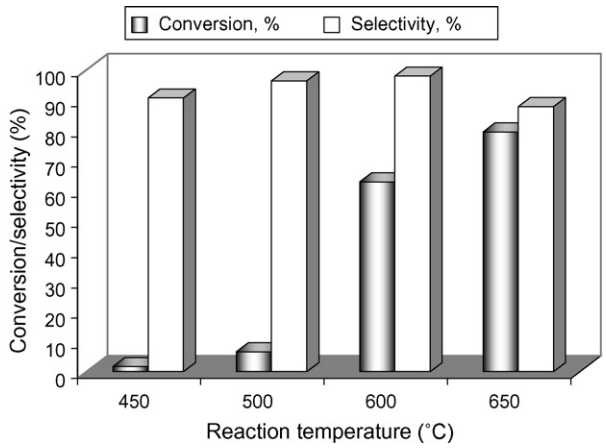

Fig. 9. Influence of reaction temperature in the EBD activity over Sn1.5Zr8.5 catalyst. Reaction conditions: catalyst weight = 1.0 g, pressure = 1 atm, CO_2/EB = 6 (molar ratio), W/F = 17.6 g_{cat} h/mol.

those are present in the isolated oxides. In other words, in Sn1.5Zr8.5 catalyst acid–base bi-functionality has been significantly increased, which has been reflected in the dehydrogenation of ethylbenzene to styrene in the presence of CO_2 as in our earlier report [15]. Furthermore, nanosize effect might be playing a role in enhancing the catalytic activity.

The catalytic activity of Sn1.5Zr8.5 at different reaction temperatures has been shown in Fig. 9. The catalytic activity of Sn1.5Zr8.5 at 450 °C is negligible, wherein, the conversion of ethylbenzene is only 2.2% and the selectivity of styrene is 89.8%. As the reaction temperature increases to 500 °C the conversion of ethylbenzene augmented, but it is not so considerable amount. At 600 °C the conversion of ethylbenzene has been attained a maximum value of 61.1% with the styrene selectivity of 97.6%. Further increase of reaction temperature to 650 °C, the conversion has been increased to 79.4%, but the selectivity of styrene has been substantially diminished. Hence, the optimum reaction temperature is 600 °C.

4. Conclusions

Preparation of SnO_2–ZrO_2 nanocomposite catalysts by simplified and environmentally acceptable conditions has been achieved. The formation of mixed oxide nanocomposite catalysts, consequent enhancement in the acid–base bi-functional behavior and the augmentation of catalytic performance for the oxidative dehydrogenation of ethylbenzene to styrene than those of single constituent oxides has been accomplished.

Acknowledgements

The authors are thankful to Inha University for the financial support and one of the authors, David Raju Burri is grateful to Korea Federation of Science and Technology for a Brain Pool fellowship. The authors also acknowledge Dr. K. Chandra Sekhar, Head Analytical Chemistry Group, DMRL, Hyderabad, for providing the elemental analysis data.

References

[1] F. Cavani, F. Trifiro, Appl. Catal. A 133 (1995) 219.
[2] T. Hirano, Appl. Catal. 26 (1986) 65.
[3] J. Matsui, T. Sodesawa, F. Nozaki, Appl. Catal. A 67 (1991) 179.
[4] W.S. Dubner, US Patent 5,276,235 (1994).
[5] R. Dittmeyer, V. Hollein, P. Quicker, G. Eming, G. Hausinger, F. Schmidt, Chem. Eng. Sci. 54 (1999) 1431.
[6] M. Sugino, H. Shimada, T. Turuda, H. Miura, N. Ikenaga, T. Suzuki, Appl. Catal. A 121 (1995) 125.
[7] N. Mimura, M. Saito, Catal. Today 55 (2000) 173.
[8] J.-S. Chang, S.-E. Park, M.S. Park, Chem. Lett. (1997) 1121.
[9] A. Sun, Z. Qin, S. Chen, J. Wang, Catal. Today 93–95 (2004) 273.
[10] T. Badstube, H. Papp, R. Dziembaj, P. Kustrowski, Appl. Catal. A 204 (2000) 153.
[11] M.-S. Park, V.P. Vislovskiy, J.-S. Chang, Y.-G. Shul, J.S. Yoo, S.-E. Park, Catal. Today 87 (2003) 205.
[12] V.P. Vislovskiy, J.-S. Chang, M.-S. Park, S.-E. Park, Catal. Commun. 3 (2002) 227.
[13] Y. Sakurai, T. Suzaki, K. Nakagawa, N. Ikenaga, T. Suzuki, Appl. Catal. A 192 (2000) 281.
[14] J.-N. Park, J. Noh, J.-S. Chang, S.-E. Park, Catal. Lett. 65 (2000) 75.
[15] D.R. Burri, K.-M. Choi, D.-S. Han, J.-B. Koo, S.-E. Park, Catal. Today 115 (2006) 242.
[16] D.R. Burri, K.-M. Choi, S.-C. Han, A. Burri, S.-E. Park, Bull. Korean Chem. Soc. 28 (2007) 53.
[17] D.R. Burri, K.-M. Choi, J.-H. Lee, D.-S. Han, S.-E. Park, Catal. Commun. 8 (2007) 43.
[18] D.R. Burri, K.-M. Choi, S.-C. Han, A. Burri, S.-E. Park, J. Mol. Catal. 269 (2007) 58.
[19] J. Ba, D.F. Rohlfing, A. Feldhoff, T. Brezesinski, I. Djerdj, M. Wark, M. Niederberger, Chem. Mater. 18 (2006) 2848.
[20] L. Jiang, G. Sun, Z. Zhou, S. Sun, Q. Wang, S. Yan, H. Li, J. Tian, J. Guo, B. Zhou, Q. Xin, J. Phys. Chem. 209 (2005) 8774.
[21] C. Lahousse, A. Abovlayt, F. Mauge, J. Bachelier, J.C. Lavelley, J. Mol. Catal. 85 (1983) 283.
[22] I. Wang, W.F. Chang, R.J. Shiau, W.C. Wu, C.C. Chung, J. Catal. 83 (1983) 428.
[23] G.W. Wang, H. Hattori, K. Tanabe, Bull. Chem. Soc. Jpn. 56 (1983) 2407.